EAST EUROPEAN JOURNAL OF PHYSICS. 4. 435-441 (2025)
DOI:10.26565/2312-4334-2025-4-43 ISSN 2312-4334

ELECTROPHYSICAL CHARACTERIZATION OF PHOTODETECTORS BASED ON SEMICONDUCTOR STRUCTURES Si (Li) AND Si(Au)

Ilhom I. Maripov[1]*, Sali A. Radzhapov[2], Sardor F. Xasanov[1], Damir B. Istamov[2], Yusuf T. Yuldashev[1], Diyora Axnazarova[3], Shamshiddin A. Ashirov[3]
[1]*Tashkent State Agrarian University, Tashkent Region, 111160, Uzbekistan*
[2]*Physical-Technical Institute of Uzbekistan Academy of Sciences, Tashkent 100084, Uzbekistan*
[3]*Gulistan State University, 4 micro districts, 120100, Gulistan, Uzbekistan*
**Corresponding Author e-mail: maripov1988@gmail.com*
Received July 9, 2025; revised October 3, 2025; accepted October 10, 2025

This paper explores the technological and physical principles for developing silicon-lithium (Si(Li)) nuclear radiation detectors with a thickness greater than 1.5 mm and a surface area of at least 50 cm^2. The formation of large-area p–i–n structures via lithium-ion drift and diffusion mechanisms was analyzed. To evaluate the electrophysical parameters of the detectors, current-voltage (I–V) and capacitance-voltage (C–V) characteristics were measured. The I–V results under reverse bias in the range of $U = 0 – 200$ V showed extremely low leakage currents $I \leq 0.5$ nA, indicating the formation of high-quality p – i – n junctions. Beyond 100 V, the current remained nearly constant, forming a plateau region. The findings propose effective technological solutions for developing highly sensitive, stable, and low-noise radiation detectors.
Keywords: *Detector; Heterostructure; Silicon; Germanium; Semiconductor p–i–n structure; p–n junction; Electrophysical properties*
PACS: 73.40. Sx, 73.61.Cw, 73.61.Ey, 72.20.Ee

INTRODUCTION

In recent years, semiconductor-based detectors have been widely applied in various fields such as nuclear physics, medical diagnostics, environmental monitoring, and cosmic radiation detection [1–5]. In particular, detectors based on semiconductor materials such as silicon (Si) and germanium (Ge) are distinguished by their high sensitivity and accuracy. The electrical and physical properties of these materials enable their effective use as radiation-responsive detectors [6-9]. This study focuses on the electrophysical and radiometric properties of detectors fabricated with $Al - nGe(p - i - n) - Au$ and $Au - nSi - Al$ structures. The $Al - nGe(p - i - n) - Au$ detector, based on germanium, exhibits high sensitivity due to the presence of a p–i–n junction. Meanwhile, the $Au - nSi - Al$ detector, based on silicon, is characterized by its low-noise operational regime. During the research, the current-voltage (I–V) and capacitance-voltage (C–V) characteristics of the detectors were analyzed, along with investigations into their radiation sensitivity, temperature dependence, and physical phenomena arising under irradiation. The results of this work contribute to the advancement of modern semiconductor detectors by enhancing their sensitivity and expanding their applicability across different technological fields [10–13]. The development of such detectors begins with a thorough study of the parameters of the materials used in their fabrication. Accordingly, we have theoretically analyzed the energetic properties of Si and Ge, the primary semiconductor materials used in this research. The analysis involved understanding the interaction between metal and semiconductor layers, as well as the variations in these properties across the material's depth. We specifically examined the physical processes occurring in these regions and evaluated their influence on the detector's performance [14–16]. In this work, we conducted an in-depth study of the electrophysical and radiometric characteristics of $Al - nGe(p - i - n) - Au$ and $Au - nSi - Al$ structures. Through this, we determined their optical and electrical parameters. Globally, the development of compact semiconductor detectors has made significant advancements. To date, detectors with dimensions of up to 50 mm based on the $Al - nGe(p - i - n) - Au$ structures have been developed by researchers worldwide. A critical aspect of $Al - nGe(p - i - n) - Au$ structured semiconductor detectors is ensuring a uniform concentration of lithium ions within a defined depth of the silicon crystal. This uniform distribution is essential for achieving optimal detector performance [17–18]. Therefore, technological processes based on diffusion and drift methods, which are widely used to introduce dopant atoms into the crystal lattice, require optimization to ensure homogeneous dopant distribution throughout the bulk of the crystal.

RESEARCH METHODOLOGY

In the development of semiconductor detectors used for recording nuclear radiation, the energy levels and potential barrier diagrams of key elements — silicon (Si) and germanium (Ge) — are of primary importance. These parameters are illustrated in Figure 1. The analysis was conducted explicitly for the detector based on the $Au - nSi - Al$ structure, and the results are presented using the corresponding energy band diagram.

Cite as: I.I. Maripov, S.A. Radzhapov, S.F. Xasanov, D.B. Istamov, Y.T. Yuldashev, D. Axnazarova, Sh.A. Ashirov, East Eur. J. Phys. 4, 435 (2025), https://doi.org/10.26565/2312-4334-2025-4-43
© I.I. Maripov, S.A. Radzhapov, S.F. Xasanov, D.B. Istamov, Y.T. Yuldashev, D. Axnazarova, Sh.A. Ashirov, 2025; CC BY 4.0 license

As shown in Figure 1, the energy transitions and theoretical energy band structure of the semiconductor material silicon (Si) are depicted. The upper part of the diagram illustrates the energy levels across the detector structure. Region No. 0 (the Au electrode) has an energy level of approximately 5.00 eV, indicating that gold (Au), due to its high work function, forms a potential barrier at the interface with silicon. This barrier makes it somewhat more difficult for electrons to move from the gold contact into the silicon region. Region No. 1 represents n-type silicon, where the bandgap energy is approximately 1.1 eV. However, in this diagram, the vertical axis indicates an energy value of around 4.20 eV. The Fermi level (indicated by the red dotted line) lies between the conduction and valence bands, but given the n-type nature of the silicon, the Fermi level is positioned closer to the conduction band. This confirms that the majority charge carriers in the n-type Si are electrons, and their preferred direction of motion is from left to right ($Au \rightarrow Al$). The energy level of the Al electrode is approximately 4.24 eV, which suggests that at the $Al - nSi$ interface, the potential barrier is relatively small – significantly lower than that at the $Au - Si$ junction. As a result, electron transport toward the Al side is more favorable in this detector. Considering that the central region of the detector is composed of n-type silicon, it can be concluded that electrons are the primary charge carriers in the device. The energy band diagram also indicates the presence of an internal electric field across the structure, which facilitates the rapid separation and collection of charge carriers under the influence of this field.

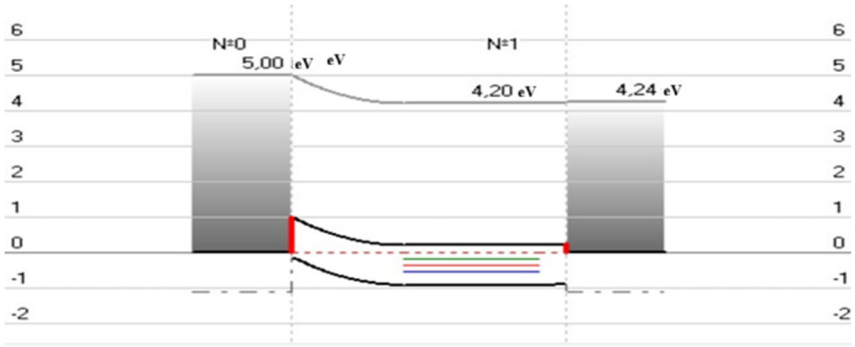

Figure 1. Energy band diagram of the $Au - nSi - Al$ structured detector based on silicon

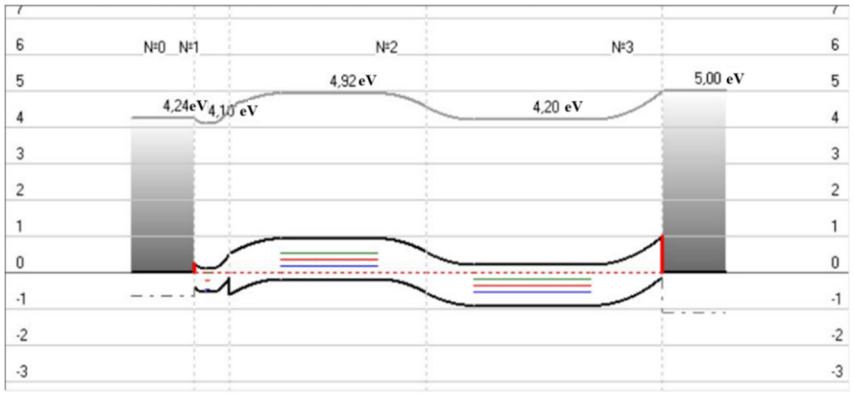

Figure 2. Energy band diagram of the $Al - pGe(p - i - n) - Au$ structured detector based on germanium

As shown in Figure 2, energy barriers, Fermi level positions (red dotted lines), and the movement of charge carriers are illustrated for each layer of the structure. $N0 \rightarrow N1$ ($Al\ contact\ to\ p - Ge$)**:** This region represents the interface between the aluminum electrode and the p-type germanium layer. The downward slope of energy barriers indicates a favorable path for electron movement. The Fermi level is located close to the valence band, confirming the p-type character of this region. $N1 \rightarrow N2$ ($p - Ge \rightarrow i - Ge \rightarrow n - Ge$) This is the core of the p–i–n structure. The energy gap of 4.92 eV corresponds to the intrinsic region of germanium. The bent portion between black lines reflects the internal potential gradient. The Fermi level is nearly centered, which is typical for intrinsic semiconductors. In this i-region, charge carriers (electron-hole pairs) are generated when photons or ionizing particles interact. $N2 \rightarrow N3$ ($n - Ge\ to\ Au$) This segment extends from the n-type Ge to the gold (Au) contact. The Fermi level lies higher, which aligns with n-type behavior. A gradual upward slope of the energy levels reflects the internal electric field generated under external bias. Under radiation exposure, the electron–hole pairs created in the i-region are quickly separated and directed towards their respective electrodes, resulting in a measurable signal. The spatial variation of the Fermi level across the layers indicates the formation of an internal electric field. Additionally, adjusting the electrode thickness allows fine-tuning of key detector parameters (Figure 2). Technological Fabrication Overview. The fabrication of $Au - nSi - Al$ and $Al - pGe(p - i - n) - Au$ semiconductor detectors for nuclear radiation detection is a complex process involving mechanical, chemical, and thermal operations, as well as precise structural design. Each step has a specific purpose and requires meticulous control. Refined

semiconductor processing technologies determine the ability of these detectors to preserve radiation sensitivity over extended periods. In this study, silicon wafers with diameters of $\theta = 10 - 30\ mm$ and thicknesses of $d = 1 - 2\ mm$ were prepared using $p - type$ monocrystalline silicon ($\rho = 0.01 - 5\ k\Omega \cdot cm, \tau = 50 - 1000\ \mu s$). The wafers were cut with a diamond internal arc saw. To remove the mechanically damaged layer, double-sided grinding was performed using M-14 and M-5 micropowders. Each side was ground to a depth of at least 50 μm. After grinding, the wafers were cleaned with non-alkaline soap and deionized water and subjected to ultrasonic treatment. The mechanical damage often exceeds the abrasive grain size, particularly when using diamond powders. Therefore, chemical etching was employed to remove residual defects. Before etching, the wafers were rinsed in distilled water for at least 15 minutes. The chemical solution was prepared using hydrofluoric acid (HF), nitric acid (HNO_3), and acetic acid (CH_3COOH) in a 1:5:1 ratio, and cooled to 5°C**.** This slow etching process allowed better control. The wafers were rotated in a fluoroplastic bath for 15–20 minutes using a motorized platform to ensure uniform surface processing. The optimal etch rate was 4 μm/min.

RESULTS AND DISCUSSION

The condition of the silicon wafers prepared for experimental research after completing the step-by-step processing stages described above is illustrated in Figure 3 (a–b–c)**.**

a) Appearance of the silicon wafer after cutting

b) Appearance of the silicon wafer after mechanical processing

c) Appearance of the silicon wafer after chemical treatment

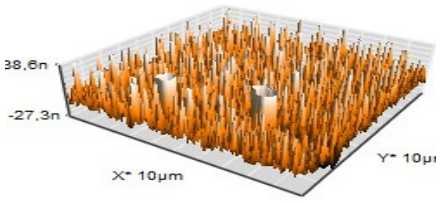

a) Appearance of the silicon wafer after cutting

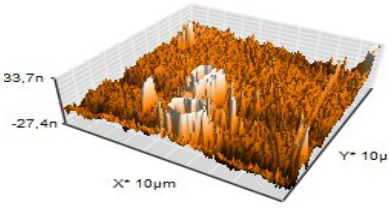

b) Appearance of the silicon wafer after mechanical processing

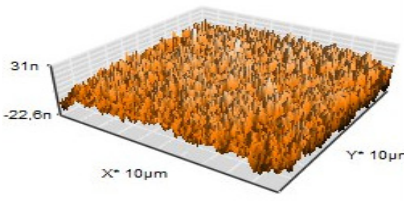

c) Appearance of the silicon wafer after chemical treatment

Figure 3 (a–b–c) shows images of the silicon wafers obtained using Atomic Force Microscopy (AFM) after the technological processing steps

As shown in Figure 3(a)**,** surface irregularities of approximately 38 nm are formed on the silicon wafer after the cutting process. In Figure 3 (b)**,** these irregularities are reduced to 33.7 nm after mechanical processing. Finally, Figure 3(c) shows that the asymmetrical layer is further reduced to 31 nm after chemical cleaning. This demonstrates the gradual decrease in surface non-uniformity through successive technological steps. Achieving high energy resolution in semiconductor detectors is one of the more complex challenges in detector development. This primarily depends on the growth technologies of the initial semiconductor materials and their electrical and structural properties. Localized defects and impurity bands in the sensitive volume significantly degrade the detector's radiometric characteristics. A key advantage of lithium-doped silicon and germanium is their ability to create large, nearly intrinsic regions exceeding 1 mm in thickness. This is made possible due to the high mobility of lithium ions in Group IV crystals and their low ionization energies – 0.033 eV in silicon and 0.0043 eV in germanium.

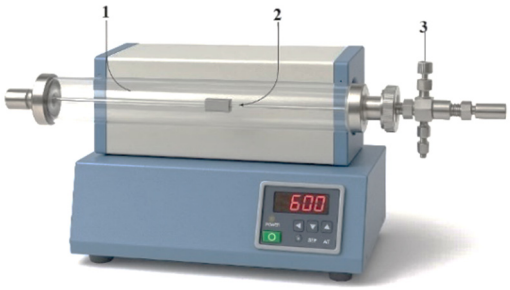

Figure 4. Schematic diagram of the device used for lithium diffusion: 1 – quartz tube, 2 – lithium sample, 3 – needle valve

For example, the diffusion coefficient of lithium in germanium is approximately 10^7 times higher than that of conventional donor atoms. Lithium ions, due to their small radius, do not occupy lattice sites but instead migrate through interstitial positions. In silicon, lithium ions form an extended intrinsic zone, which significantly enhances sensitivity to X-rays and gamma radiation**.** This region generates a high-resistance volume inside the crystal, facilitating charge collection and signal generation within the detector. To implement lithium diffusion in small-sized crystals, a GSL-1100X furnace was

used. The furnace consists of a quartz tube for sample placement. Diffusion was performed across the entire surface of the wafers at a vacuum of ~10^{-5} mmHg**,** to a depth of (50–200) μm**,** for 1 to 3 minutes, at temperatures between 380°C and 450°C **(**Figure 4**)**. After diffusion, the crystals were slowly cooled to 250°C to prevent defect formation and lithium ejection, which typically occurs during rapid cooling. Diffusion depth was controlled using a step-grinding technique**.** The depth of lithium diffusion into p-type silicon can be determined using the following formula:

$$x_j = 2\sqrt{Dt}\ erfc^{-1}\left(\frac{N_A}{N_0}\right) \tag{1}$$

Here, D is the diffusion coefficient, which is calculated for p-type silicon with a specific resistivity of approximately $\rho \approx 1000\,\Omega \cdot cm$, as follows:

$$D = 6 \cdot 10^{-4} \exp\left(\frac{-0{,}61\,q}{k_B T}\right)\left[cm^2/s\right] \tag{2}$$

Here, q is the elementary charge, k_B is the Boltzmann constant and T is the temperature in Kelvin.

In p-type material, compensation of acceptor atoms through lithium diffusion is carried out as follows: First, lithium is directed into the p-type material. The temperature is then raised to approximately 430 °C**,** initiating the diffusion of lithium into the sample. The diffusion process lasts for several minutes, during which lithium penetrates to a depth of approximately 0.01 μm. Subsequently, lithium ions begin to migrate from the n-side back toward the p-side of the p–n junction. In this region, they compensate for the acceptor atoms present in the p-type material. The thickness of the depleted layer formed as a result of this diffusion process can be calculated using the following formula:

$$d = \sqrt{2\mu_{Li} U t}, \tag{3}$$

Here, d is thickness of the depleted layer, μ_{Li} is the ion mobility in semiconductors at the given diffusion temperature, U is the drift bias voltage and t is the drift time.

The diffusion time is determined as follows:

$$t = \frac{W^2}{2U\mu_{Li}}, \tag{4}$$

Here, W is the thickness (width) of the compensated intrinsic (i) region in the Si(Li) detector.

The relationship between mobility and the diffusion coefficient is as follows:

$$\mu_{Li} = \frac{q}{k_B T} \cdot D\left[sm^2/(V \cdot s)\right] \tag{5}$$

The thermal regime of lithium-ion drift is described in detail to ensure the required compensation at minimal redistribution of the lithium profile within the sensitive volume.

Drift was performed unidirectionally at a temperature of T = (60–100)°*C*, under a reverse bias voltage of 70–600V, for a duration of four days. The completion of the drift process was monitored by a sharp increase in the reverse current. To determine the i-region, after drift termination, one side of the crystal (with an $n^+ - i - p^+$ structure) was polished using silicon carbide (SiC) micro powder on a glass disc. The thickness of the removed layer was estimated considering partial washout of the diffusion profile. The polished layer typically had a thickness ranging from 50 to 400 μm**.** The i-region was then selectively removed using an etching solution of HNO_3:HF in a 1:1000 ratio**.** The i-region was considered entirely removed when its contour matched the diameter of the diffused region and appeared close to a circular shape.

The geometry of Si(Li) p–i–n detectors play an important role in determining their electrical and detection characteristics. Two typical structural configurations are illustrated in Figure 5: the planar geometry (Figure 5a), where the p–i–n layers extend uniformly across the detector surface, and the T-type reference geometry (Figure 5b), which is widely used to reduce surface leakage currents and improve charge collection efficiency. The key design parameters include the detector diameter (D), the thickness of the intrinsic (i) region (d), the thickness of the p-region (h), and the diameter of the n-region (2r).

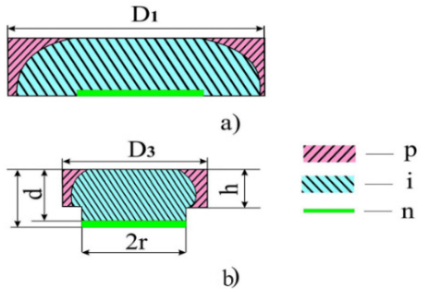

Figure 5. Cross-sectional view of the detector: a – planar, b – T-type reference geometry
D – detector diameter; d – thickness of the intrinsic (i) region; h – thickness of the p region; 2r – diameter of the n region.

It should be emphasized that when performing diffusion doping of silicon, it is essential to consider the thermal and temporal regimes to avoid the formation of thermally induced defects. In the technology of Si(Li) p–i–n detectors, lithium is typically diffused at temperatures ranging from 300°C to 500°C, with a critical threshold at 450°C**,** beyond which the intensive generation of donor-type thermodefects occurs. In known Si(Li) p–i–n detector fabrication processes, a rapid cooling step is applied after diffusion to preserve the desired lithium profile and prevent redistribution. However, this high cooling rate (on the order of 10^2–10^3 °C/s) can induce stable thermodefects, which may negatively affect the final characteristics of the semiconductor detector. The formation of electrical contacts on the prepared silicon wafers was carried out using a VPS-4 universal vacuum post system. The sample holders were specially designed using molybdenum and tungsten, cleaned in alcohol, and then preheated in a vacuum for 10–15 minutes**.** The molybdenum filament had a length of 40 mm, and the distance between the evaporator and the silicon wafer was set at 80 mm**.** The silicon wafers were placed in the evaporation chamber, and contacts were deposited under a vacuum of 5×10^{-5} mmHg. As a contact material, gold layers with a thickness of approximately 200 Å were deposited on the silicon wafers.

The visual appearance of the silicon wafers before and after contact formation is shown in Figure 6. In particular, Figure 6a illustrates the surface morphology of the Si(Li) wafer after the lithium drift process, whereas Figure 6b demonstrates the post-diffusion appearance of the Au-coated silicon wafer. This comparison highlights the transition from the initial lithium-compensated structure to the final detector surface with gold contact deposition.

Figure 6. Appearance of the detector after contact formation
a) Post-drift appearance of Si(Li), b) Post-diffusion appearance of Si(Au)

The current–voltage (I–V) characteristics of Si(Li) p–i–n structured detectors were investigated in accordance with the GOST 26222-86 standard methodology. To study the characteristics mentioned above, a specialized device was developed and assembled for measuring reverse current, which allows for the simultaneous acquisition of dark current values across different bias conditions. The applied reverse bias voltage $U_{rev.}$was set in the range of 0.1 to 800 V, and the current measurement ranges $I_{rev.}$ were configured for 1 μA**,** 10 μA**,** and 100 μA**,** respectively.

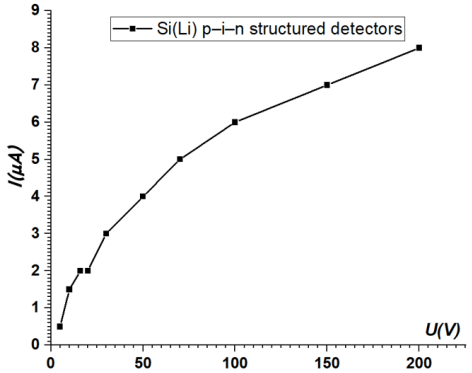

Figure 7. Current–voltage (I–V) characteristics of semiconductor Si(Li) p–i–n structured detectors

Figure 7 illustrates the dependence of the output current. I_{output} on the output voltage U_{output} for a detector with a T-shaped cross-section, showing both the minimum and maximum current values. As shown in the graph, the output current across the entire detector volume ranges from 0.5 to 9 μA at an applied voltage of 200 V.

This indicates that a uniform compensation has been achieved within the silicon volume (30 mm in diameter and 2 mm in thickness) by lithium ions. As the voltage increases, the current also rises; however, this increase is non-linear and gradually approaches a saturation-like regime. In the initial voltage region (0–30 V), the current increases sharply with voltage, indicating the onset of the drift process. In this zone, the detector exhibits high sensitivity. In the intermediate region (30–100 V), the growth of the current slows down. This suggests that the drift region is expanding, although a significant portion of the lithium ions in the silicon has already been positioned. At high voltages (100–200 V and beyond), the current increase becomes nearly negligible and deviates significantly from linearity, indicating saturation. This means the drift layer has reached its maximum extent, and the detector operates in a stable regime at these voltages. It is well known that capacitance-voltage **(**C–V) characteristics can be used to determine both the density of surface states and their distribution function across the energy bandgap at the semiconductor–dielectric interface of monocrystalline silicon. Several methods have been developed to analyze these parameters based on C–V measurements.

It is well established that capacitance–voltage (C–V) characteristics provide valuable insights into the density of surface states and their energy distribution at the semiconductor–dielectric interface. This type of C–V analysis is particularly significant for evaluating the physical - parametric properties of $Si(Li)$ –based detectors**.** Figure 8 presents the C–V characteristic of an $Al - nGe(p - i - n) - Au$ detector, which is based on a $p - i - n$ (positive–intrinsic–negative) type semiconductor structure. In such detectors, due to the narrow width of the intrinsic (i) layer, the depletion region extends significantly**,** resulting in a low overall capacitance. As the applied voltage increases, the capacitance decreases slowly. The C–V curve generally shows a downward trend with increasing bias voltage, ultimately reaching a plateau region where the capacitance becomes nearly constant. From the graph, it can be observed that in the initial voltage range (~0–20 V)**,** the capacitance decreases rapidly, indicating the expansion of the depletion region**.** In the 30–35 V range, a plateau forms, indicating that the structure has reached complete depletion, and further increase in voltage no longer significantly affects the capacitance. The capacitance starts at approximately 300 pF and stabilizes as it approaches the plateau. Under this condition of complete depletion**,** the detector yields a clean and well-defined signal, indicating its optimal operating state. Any additional voltage serves only to stabilize the operation and does not affect the capacitance further. On the other hand, the $Au - nSi - Al$ detector features a structure based on a classical n-type semiconductor (Si) and behaves similarly to a Schottky barrier or p–n junction detector. In this case, applying a voltage causes the depletion region to deepen, but since there is no intrinsic layer (i-region), the capacitance remains relatively high. Consequently, the C–V characteristic of such detectors exhibits a steeper and more abrupt decrease. Due to the shorter depletion width, the capacitance begins at a higher level (approximately 300–400 pF) and decreases rapidly as the voltage increases. The $C = f(V)$ graph for this detector type shows a rapid drop in capacitance with little to no observable plateau.

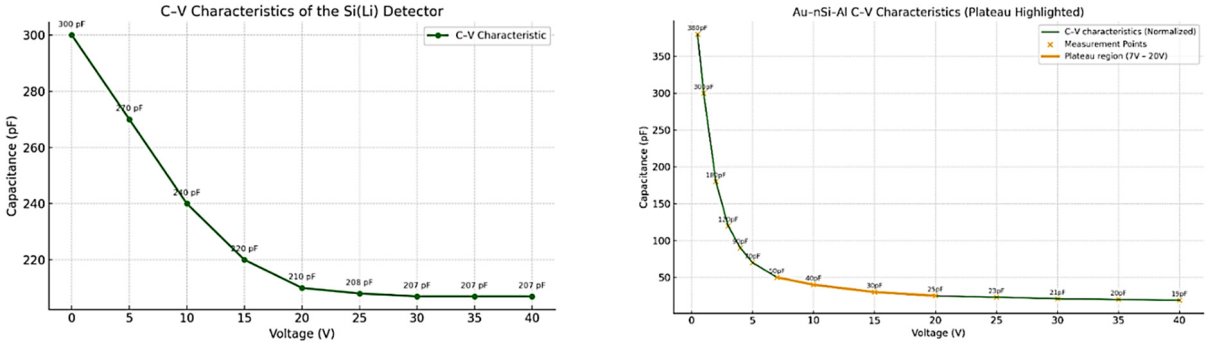

a) b)

Figure 8. Capacitance-voltage $(C - V)$ characteristics
a) $Al - nGe(p - i - n) - Au$. b) $Au - nSi - Al$ detectors

The capacitance-voltage (C–V) characteristics were studied using the E7-12 instrument at a frequency of 1 MHz**,** and a modernized L2-7-1M instrument was employed for measurements in the 0.465 MHz to 10 MHz frequency range. These instruments ensured that the amplitude of the applied AC signal did not exceed 5–7 mV. All measurements were carried out at a temperature of T = 300 K, using both parallel and series equivalent circuit configurations. The measurement error did not exceed 0.1pF. The voltage-capacitance characteristics investigated for detectors of different types demonstrate that a high compensation quality was achieved during fabrication, owing to the drift process of lithium ions within the detector material.

The obtained results are considered to be optimal for semiconductor detectors. Consequently, through investigations and technological processes, the fabrication technology of $Si(Li)$ –based semiconductor detectors with a $p - i - n$ structure has been developed and optimized.

CONCLUSIONS

The choice of detector material and structure directly affects their electrophysical and radiometric properties. In particular, detectors with a $p - i - n$ structure stands out from other types due to their high resolution and low current noise. High sensitivity and stability were achieved in low-defect p-type silicon (pSi) samples due to deep lithium diffusion. The high resistance and extremely low leakage current of the detector demonstrated its excellent energy resolution capability. Measurements of detectors based on the $Au - nSi - Al$ structure showed that this type of detector has greater radiation tolerance, making it suitable for continuous operation. The capacitance–voltage (C–V) and current-voltage (I–V) characteristics were measured for both types of detectors, revealing that the depletion region is fully formed within the voltage range of 30 – 35 V. The plateau region observed in the C–V characteristics indicates full activation of the detector, while the low current observed under reverse bias in the I–V characteristics confirms the formation of a high-quality p–n junction. These detectors have high potential for use in various applications, including cosmic radiation detection, nuclear medicine, environmental monitoring, and security systems.

ORCID

Ilhom I. Maripov, https://orcid.org/0009-0005-1683-2260

REFERENCES

[1] E. Fortunato, M. Vieira, L. Ferreira, *et al*. "Large Area Position Sensitive Detector Based on Amorphous Silicon Technology," MRS Online Proceedings Library, **297**, 981–986 (1993). https://doi.org/10.1557/PROC-297-981

[2] D. Protić, T. Krings, and R**.** Schleichert, "Development of double-sided microstructured Si(Li) detectors," IEEE Transactions on Nuclear Science, **49**(4), 1829–1832 (2002). https://doi.org/10.1109/TNS.2002.801541

[3] J. Wang, P. Mulligan, L. Brillson, and L.R. Cao, "Review of using gallium nitride for ionizing radiation detection," Applied Physics Reviews, **2**(3) 031102 (2015). https://doi.org/10.1063/1.4929913

[4] Z. Xie, K. Jiang, S. Zhang, Z. Wang, X. Shan, B. Wang, and J. Ben, *et al*. "Ultraviolet Optoelectronic Synapse Based on AlScN/p-i-n GaN Heterojunction for Advanced Artificial Vision Systems," Advanced Materials, **37**(19), e2419316 (2025). https://doi.org/10.1002/adma.202419316

[5] A. Keffousa, M. Siad, A. Cheriet, N. Benrekaa, Y. Belkacem, H. Menari, W. Chergui, and A**.** Dahmani, "Comparison of electrical and optical parameters of Au/n-Si and Ag/n-Si Schottky barrier photodiodes,". Applied Surface Science, **236**(1–4), 42-49 (2004). https://doi.org/10.1016/j.apsusc.2004.03.233

[6] M. Kozai, H. Fuke, M. Yamada, K. Perez, T. Erjavec, C. J. Hailey, N. Madden, *et al*. "Developing a mass-production model of large-area Si(Li) detectors with high operating temperatures," Nuclear Instruments and Methods in Physics Research Section A: Accelerators, Spectrometers, Detectors and Associated Equipment, **947**, 162695 (2019). https://doi.org/10.1016/j.nima.2019.162695

[7] R.A. Muminov, A.K. Saymbetov, N.M. Japashov, Y. Toshmurodov, S.A. Radzhapov, N.B. Kuttybay, and M.K**.** Nurgaliyev, "Physical Features of Double Sided Diffusion of Lithium into Silicon for Large Size Detectors," Journal of Nano- and Electronic Physics, **11**(2), 02031-1–4 (2019). https://doi.org/10.21272/jnep.11(2).02031

[8] J. Grant, C. Buttar, M. Brozel, A. Keffous, A. Cheriet, K. Bourenane, A. Bourenane, *et al*. "Lithium-drifted, silicon radiation detectors for harsh radiation environments," Journal of Materials Science: Materials in Electronics, **19**(S1), S14–S18 (2008). https://doi.org/10.1007/s10854-008-9707-0

[9] D. Alexiev, M.I. Reinhard, L. Mo, A. R. Rosenfeld, and M. L. Smith, "Review of Ge detectors for gamma spectroscopy," Australasian Physics & Engineering Sciences in Medicine, **25**(3), 102–109 (2002). https://doi.org/10.1007/BF03178770

[10] A. Keffous, M. Siad, A. Cheriet, Y. Belkacem, H. Menari, W. Chergui, and A. Dahmani, "Effect of the lithium diffusion into n-type silicon on the spectral response of the Schottky photodiodes," Optics Communications, **222**(4–6), 299–304 (2003). https://doi.org/10.1016/S0030-4018(03)01604-3

[11] M. Xiao, A. Stoessl, B. Roach, C. Gerrity, I. Bouche, G. Bridges, P. von Doetinchem, *et al*. "Large-Scale Detector Testing for the GAPS Si(Li) Tracker," IEEE Transactions on Nuclear Science, **70**(8), 2125-2133 (2023). https://doi.org/10.1109/tns.2023.3291235

[12] D.B. Istamov, O.A. Abdulkhayev, and Sh.M. Kuliyev, "Limiting characteristics of silicon diode temperature sensors for determining the maximum temperature with specified measurement accuracy," UNEC J. Eng. Appl. Sci. 5(1), 63-69 (2025). https://doi.org/10.61640/ujeas.2025.0507

[13] D.B. Istamov, O.A. Abdulkhayev, Sh.M. Kuliyev, N. Abdullayev, A.Sh. Ashirov, and D.M. Yodgorova, "Temperature response curve of silicon diode temperature sensors," East Eur. J. Phys. (2), 287-291 (2025), https://doi.org/10.26565/2312-4334-2025-2-35

[14] R.R. Bebitov, O.A. Abdulkhaev, D.M. Yodgorova, D.B. Istamov, G.M. Hamdamov, Sh.M. Kuliyev, A.A. Khakimov and A.Z. Rakhmatov, "Dependence of the accuracy of the silicon diode temperature sensors for cryogenic thermometry on the spread of their parameters," Low Temperature Physics, **49**(2), 277–282 (2023). https://doi:10.1063/10.0016843

[15] R.R. Bebitov, O.A. Abdulkhaev, D.M. Yodgorova, D.B. Istamov, Sh.M. Kuliyev, A.A. Khakimov, A.B. Bobonazarov, *et al*. "Distribution of impurities in base-depleted region of diode temperature sensor," Low Temperature Physics, **50**(5), 418–424 (2024). https://doi.org/10.1063/10.0025635.

[16] I.M. Isakovich, O. S. Komilovich, and M. F. Gallievna, "Electrophysical Properties of Al-pGe(p-i-n)-Au and Au-nSi-Al Structural Detectors Prepared on the Basis of Si and Ge," Physical and mathematical sciences, (2), 23-29 (2024). https://doi.org/10.24412/2709-1201-2025-28-23-29

[17] J. Grant, C. Buttar, M. Brozel, A. Keffous, A. Cheriet, K. Bourenane, A. Bourenane, *et al*. "Lithium-drifted, silicon radiation detectors for harsh radiation environments," J. Mater. Sci: Mater. Electron. **19**, S14–S18 (2008). https://doi.org/10.1007/s10854-008-9707

[18] W.R. Leo, *Techniques for Nuclear and Particle Physics Experiments*, (Springer-Verlag Berlin Heidelberg GmbH, 1994). https://doi.org/10.1007/978-3-642-57920-2

ЕЛЕКТРОФІЗИЧНА ХАРАКТЕРИЗАЦІЯ ФОТОДЕТЕКТОРІВ НА ОСНОВІ НАПІВПРОВІДНИКОВИХ СТРУКТУР Si(Li) ТА Si(Au)

Ілхом І. Маріпов[1], Салі А. Раджапов[2], Сардор Ф. Хасанов[1], Дамір Б. Істамов[2], Юсуф Т. Юлдашев[1], Діора Ахназарова[3], Шамшіддін А. Аширов[3]

[1]Ташкентський державний аграрний університет, Ташкентська область, 111160, Узбекистан
[2]Фізико-технічний інститут Академії наук Узбекистану, Ташкент 100084, Узбекистан
[3]Гулістанський державний університет, 4-й мікрорайон, 120100, Гулістан, Узбекистан

У цій статті досліджено технологічні та фізичні принципи створення ядерних детекторів випромінювання на основі кремній-літієвих (Si(Li)) структур із товщиною понад 1,5 мм та площею поверхні не менше 50 см². Аналізується формування великогабаритних p–i–n структур шляхом дрейфу та дифузії іонів літію. Для оцінки електрофізичних параметрів детекторів були проведені вимірювання вольт-амперних (I–V) та ємнісно-напругових (C–V) характеристик. Результати I–V при зворотному зміщенні в діапазоні U = 0–200 В показали надзвичайно низькі струми витоку (I ≤ 0,5 нА), що свідчить про формування високоякісних p–i–n переходів. При напрузі понад 100 В струм залишався практично сталим, утворюючи плато. Отримані результати пропонують ефективні технологічні рішення для розробки високочутливих, стабільних детекторів випромінювання з низьким рівнем шуму.

Ключові слова: *детектор; гетероструктура; кремній; германій; напівпровідникова p–i–n структура; p–n перехід; електрофізичні властивості*